Raytheon

SEA ICE AGE / EDGE MOTION

VISIBLE/INFRARED IMAGER/RADIOMETER SUITE ALGORITHM THEORETICAL BASIS DOCUMENT

Version 3: May 2000

Igor Appel
Ken Jensen

William Emery, Science Team Member
University of Colorado

RAYTHEON SYSTEMS COMPANY
Information Technology and Scientific Services
4400 Forbes Boulevard
Lanham, MD 20706

SBRS Document # Y2409

NPOESS COMPETITION SENSITIVE

EDR: SEA ICE AGE / EDGE MOTION

Doc No: Y2409

Version: 3

Revision: 0

	Function	Name	Signature	Date
Prepared by	EDR Developer			
Approved by	Relevant IPT Lead			
Approved by	Chief Scientist	P. ARDANUY		
Released by	Program Manager	H. BLOOM		

TABLE OF CONTENTS

Page

LIST OF FIGURES

LIST OF TABLES

GLOSSARY OF ACRONYMS

AMSR	Advanced Microwave Scanning Radiometer
ARM	Atmospheric Radiation Measurement
ATBD	Algorithm Theoretical Basis Document
AVHRR	Advanced Very High Resolution Radiometer
BRDF	Bidirectional Reflectance Distribution Function
CMIS	Conical Scanning Microwave Imager/Sounder
CrIS	Cross-Track Infrared Sounder
EDR	Environmental Data Record
FIRE-ACE	First ISCCP Regional Experiment–Arctic Cloud Experiment
GCM	General Circulation Model
IORD	Integrated Operational Requirements Document
ISCCP	International Satellite Cloud Climatology Project
LUT	Look Up Table
MAS	MODIS Airborne Simulator
MCC	Maximum Cross Correlation
MESMA	Multiple Endmember Spectral Mixture Analysis
MODIS	Moderate Resolution Imaging Spectroradiometer
NPOESS	National Polar-Orbiting Operational Environmental Satellite System
NPP	NPOESS Preparatory Program
RMS	Root Mean Square
SAR	Synthetic Aperture Radar
SDR	Sensor Data Record
SHEBA	Surface Heat Budget of the Arctic Ocean
SMA	Spectral Mixture Analysis
SRD	Sensor Requirements Document
TBD	To Be Determined
TBR	To Be Reviewed
TOA	Top of Atmosphere
VIIRS	Visible/Infrared Imager/Radiometer Suite
WINCE	Winter Cloud Experiment

ABSTRACT

This Sea Ice Age and Edge Motion Algorithm Theoretical Basis Document describes the background, theory, and analysis of an algorithmic approach that can be used to develop operational algorithms to retrieve sea ice age and sea ice edge motion automatically on a global basis from Visible-Infrared remote sensing data. The data will be in the form of Sensor Data Records (SDRs) produced by the National Polar-Orbiting Operational Environment Satellite System (NPOESS) Visible/Infrared Imager/Radiometer Suite (VIIRS). Fully automated global retrievals of sea ice data from Vis-IR will be of great value to operational ice centers in the NPOESS era, especially if the VIIRS results can be combined with passive microwave results from NPOESS/CMIS.

Our process to create Sea Ice Age and Edge Motion Environmental Data Records (EDRs) from the VIIRS data has been developed to satisfy the requirements of the VIIRS Sensor Requirements Document (SRD), Version Two, Revision a. This document covers all sea ice age and edge motion processing. In particular, it describes algorithms for discrimination of Multi-year from First Year ice, nighttime and daytime dicrimination of New/Young from other First Year ice types, and retrieval of ice edge motion. The algorithms of sea ice age and sea ice edge motion retrieval have changed since the version 2 ATBD. This document describes the theoretical basis and development process of the algorithm to retrieve both sea ice age and edge motion, as required by the VIIRS SRD.

The content of the Sea Ice Age EDR is the typing of areas of sea ice by age. In practice, ice types are characterized by stage of development. Stage of development, ice age, and ice thickness represent different sides of the same thermodynamic process—ice growth. Stage of development is a standard and most commonly used parameter describing the formation and growth of ice cover. The VIIRS SRD requires that sea ice age be classified as First Year or Multi-year at a horizontal cell size of 3 km under clear conditions with a 70% probability of correct typing. Objective requirements are to distinguish also between New, Young, and First Year ice, with a 90% probability of correct typing.

Our algorithm classifies ice type by using three methods:

(1) Nighttime discrimination of New/Young ice from thicker First Year and Multi-year ice is achieved by an energy balance derivation of ice thickness from ice temperature.

(2) Daytime discrimination of New/Young ice from thicker First Year and Multi-year ice is achieved by application of a reflectance threshold.

(3) Multi-year ice is distinguished from First Year ice by a filtered distribution of ice reflectance (daytime) or ice temperature (nighttime).

All three methods use ice surface reflectance and ice surface temperature derived from VIIRS data. Different ice types exhibit both different albedo and different surface temperature. This physical basis is used for discrimination between New/Young and First Year/Multi-year ice

types. The use of reflectances of visible and near-infrared bands and ice surface temperature is an effective way to retrieve ice type for relatively thin ice cover.

Cloud contamination and snow cover have been impediments to a reliable global retrieval of ice age. Our approach relies on effective operational cloud masking from the VIIRS automated Cloud Mask algorithm to mask areas contaminated by cloud cover. Our retrievals will be performed only over clear areas. The effects of snow cover have been considered in our performance analysis, which suggests that our specifications can be attained for most cases.

Older ice tends to be colder in the winter, allowing for age classification from surface temperature. Regional and seasonal ice conditions can be used in an energy balance model, along with observed temperature to calculate ice thickness. The incorporation of air temperature (and snow depth) as ancillary data will improve the accuracy of calculations, using an energy balance model. We propose the development of LUTs that are planned to be used to transform calculated ice thickness into ice age. Classification of ice types on the basis of surface reflectance is a straightforward process. We also recommend the development of regional LUTS to transform retrieved ice surface reflectance into ice age.

The algorithm for First Year Multi-year classification takes into account features of spatial changes in ice characteristic values in a local region under consideration. Those characteristics are surface reflectance at daytime and surface temperature at nighttime. Our approach to First Year Multi-year ice classification is based on using iterative procedures involving application of a spatial filter, identification of principal peaks in probability densities (corresponding to ice classes), and segmentation. This approach has been used to successfully isolate ice age classes with synthetic aperture radar data (RADARSAT).

Sea ice edge motion is defined as the displacement of a sea ice edge. The definition of sea ice edge, taken from the VIIRS Imagery EDR, is the boundary between regions containing greater than 0.1 ice concentration and regions containing less than 0.1 ice concentration. A vector is provided for each horizontal cell containing a portion of the ice edge boundary. This vector is an estimate of the magnitude and direction of the motion of the boundary. The requirements specify that ice edge motion should be determined with a measurement uncertainty of 1 km/day, roughly equivalent to 1.15 cm/s.

The motion of the sea ice edge is determined by ice drift in the marginal ice zones. Our approach is based on the determination of the motion of ice features. The Lagrangian displacement of the features is calculated using the Maximum Cross Correlation (MCC) technique. This is a robust, widely used, and reliable technique that has been recommended for different applications.

Our modification of MCC consists of the consideration of two-dimensional fields of ice concentration, instead of the traditional use of radiance, reflectance, or surface temperature. A concentration value is derived for each VIIRS pixel, making an ice concentration image of the marginal ice zone. Spatially co-registered ice concentration image pairs are used as input for MCC. The use of ice concentration makes our approach consistent, as the location of sea ice edge boundary will be derived from the sea ice concentration retrieval also. The developed

modification of Maximum Cross Correlation (MCC) method allows us to determine the displacement of ice between its two sequential positions in a straightforward way to meet requirements. Ice edge motion vectors are computed by a weighted interpolation of all ice motion vectors within a specified distance from an ice edge location.

Cloud cover is the greatest hindrance to operational retrieval of ice edge motion. As with ice age, we rely on the VIIRS Cloud Mask, and apply MCC to clear areas only. This approach is reliable, but it necessarily will limit the amount of image pair data available for the MCC. Fortunately, the extensive monitoring of polar regions by NPOESS, with 42 orbits per day, will provide unprecedented opportunities for MCC of Visible-IR images. For cases where a recent VIIRS image is not available to correlate with the current VIIRS image, a recent CMIS image can be used.

This document presents the algorithm theoretical basis, the input data requirements, the EDR performance specification and error analysis, conditions under which the specification can not be attained, and the plan for initialization and validation. This document is version 3 of the Imagery ATBD. It is intended to completely supersede previous versions.

1.0 INTRODUCTION

1.1 PURPOSE

This Algorithm Theoretical Basis Document (ATBD) explains the mathematical background to derive the Environmental Data Record (EDR) Sea Ice Age/Edge Motion. In addition, this document provides an overview of the required input data, the physical theory, assumptions and limitations, and a performance analysis of the described algorithm. The one EDR described in this document is part of the NPOESS/VIIRS team software package of 29 EDRs.

Sea Ice Age / Ice Edge Motion algorithms consist of four major components:

(1) Discrimination of New/Young ice from thicker First Year and Multi-year ice at nighttime on the basis of an energy balance using ice surface temperature.

(2) Discrimination of New/Young ice from thicker First Year and Multi-year by application of a reflectance threshold.

(3) Discrimination of Multi-year ice from First Year ice using a filtered distribution of ice reflectance (daytime) or ice temperature (nighttime).

(4) Determination of Ice Edge Motion on the basis of applying of the Maximum Cross Correlation method to sequential images of ice concentration

1.2 SCOPE

This document covers the theoretical basis for the derivation of the EDR Sea Ice Age/Edge Motion. The purpose and scope of this document are described in Section 1 while Section 2 gives an overview of the retrieval objectives. Section 3 describes the algorithm, its input data, the theoretical background, the EDR performance analysis, error budget, and plans for initialization and validation. Section 4 lists assumptions and limitations. Section 5 contains a list of referenced publications.

1.3 VIIRS DOCUMENTS

This document contains references to other Raytheon VIIRS documents, which are given in italicized brackets. The VIIRS documents cited in this document are listed below:

[PRF SS 154640-001]	VIIRS System Specification
[PRF PS 154640-101]	VIIRS Sensor Specification
[Y2401]	Snow Cover/Depth ATBD
[Y2404]	Fresh Water Ice ATBD
[Y2405]	Ice Surface Temperature ATBD
[Y2411]	Atmospheric Correction over Land ATBD
[Y2412]	Cloud Mask ATBD
[Y2466]	Imagery ATBD
[Y2470]	VIIRS Interface Control Document
[Y2477]	VIIRS Snow/Ice Module Level Software Architecture document
[Y3258]	Earth Location ATBD

1.4 REVISIONS

This is the third version of this document, dated May 2000. The first two versions were developed in response to VIIRS Sensor Requirements Document (SRD), revision 1, dated August 3, 1998. The first version was dated October 1998. The second version was dated June 1999.

Changes since version 2 include:

- Development of an algorithm to discriminate Multi-year ice from First Year ice using a filtered distribution of ice reflectance (daytime) or ice temperature (nighttime)
- Determination of Ice Edge Motion by application of the Maximum Cross Correlation method to sequential images of ice concentration
- Replacement of a multiple endmember spectral mixture analysis (MESMA) technique with discrimination of New/Young ice from thicker First Year and Multi-year by application of a reflectance threshold
- Improvement to the error analysis and error budget, with additional tests

2.0 EXPERIMENT OVERVIEW

2.1 OBJECTIVES OF THE RETRIEVAL

The polar oceans comprise approximately 6.5% of the Earth's surface and are covered by sea ice at some time during the course of the annual cycle. At its maximum extent, sea ice blankets ~19 x 10^6 km^2 of the Southern Hemisphere and ~14 x 10^6 km^2 of the Northern Hemisphere. In the Arctic, nearly half of the late-winter maximum of sea ice cover survives the summer melt season and is classified as Multi-year ice. The net export of Multi-year sea ice through the Fram Strait is balanced by production of Multi-year ice in the Arctic basin. In the Antarctic, more than 90% of the sea ice that forms and grows in the austral winter will melt during the austral spring and summer, and as such is classified as First Year ice.

Long-term trends in the extent of sea ice can be a valuable indicator of global climate change. This is particularly true for the polar ice pack, which is believed to be sensitive to global warming, but is too remote for comprehensive *in situ* monitoring.

2.1.1 Objectives of the Sea Ice Age Retrieval

Sea ice age is defined as the time that has passed since the formation of the surface layer of an ice covered region of the ocean. The content of the Sea Ice Age EDR is the typing of areas of sea ice by age. The definition of ice age is intended to apply to the actual age of the ice that happens to be at a particular location. It is not intended to mean the time interval that has passed since ice first formed at that spot. The definition of ice age implies a synoptic description of ice type redistribution.

The heat budget of the polar regions is significantly affected by the presence of sea ice and by its annual cycle of growth and decay. Sea ice significantly inhibits the vertical flux of latent and sensible heat from the ocean to the atmosphere and reflects a large fraction of the incident solar radiation. There is a dramatic increase in surface albedo as ice forms and grows. The insulating properties of sea ice are strongly dependent on its thickness, which is directly linked to its age (Yu and Rothrock, 1996). Information on the extent of various ice age types is necessary for accurate general circulation models (GCMs) in the polar regions. GCMs do not simulate the Arctic climate very well (Bromwich and Tzeng, 1994), indicating the need to improve measurements of the global cover of sea ice of various age types. Information about ice age is also important for commercial and military operations in polar seas.

The content of the sea ice age EDR is the typing of areas of sea ice by age. In practice, ice types are characterized by stage of development. Stage of development, ice age, and ice thickness represent different sides of the same thermodynamic process—ice growth—but their meaning is different. Variability in ice thickness, to a great degree, depends upon location, climatic conditions, and season. Changes in these conditions will lead to a different rate of ice growth and quite different ice thickness achieved for the same period of time after ice formation. Our interpretation of the IORD is that stage of development of ice cover is of greater interest for Arctic and Antarctic operations and research than is the actual time that has passed since the formation of ice. Stage of development is included in the international system of sea-ice symbols and routinely used in ice charts. It is a standard and most commonly used parameter describing the formation and growth of ice cover.

Our algorithm will provide information on stage of development (i.e. ice age) for a horizontal cell, to meet SRD requirements.

The objective of the retrieval is to achieve the performance specifications designed to meet the requirements stated in the VIIRS Sensor Requirements Document (SRD). The requirements for both Sea Ice Age and Sea Ice Edge Motion are presented in a common table in the VIIRS SRD, though the algorithms are distinct.

2.1.2 Objectives of the Sea Ice Edge Motion Retrieval

Sea ice edge motion is defined in the VIIRS SRD as the displacement of a sea ice edge. An ice edge is defined in the VIIRS SRD as the boundary between regions containing ice concentration less than 0.1 and regions containing concentration greater than 0.1. We have adopted the following interpretation of the requirement: "The required EDR is a vector field defined only along ice boundaries. A vector is provided for each horizontal cell containing a portion of the boundary. This vector is an estimate of the magnitude and direction of the motion of the boundary."

The ice edge generally occurs between the ice-free ocean and the contiguous pack ice although complex patterns of ice concentration may be found, defying such simple interpretations. The advance and retreat of the ice edge during the annual cycle, creates a seasonally migrating contrast zone between the open ocean and the contiguous pack ice. This zone influences atmospheric and oceanic circulation patterns, affecting the development of local and regional weather patterns. In addition, the ice edge can move tens-of-kilometers per day in response to changes in weather conditions, significantly disrupting operational activities on the sea surface (Loset and Carstens, 1996). Ice edge boundaries are used for navigational planning, can change fast (Loset and Carstens, 1996), and so must be available in a short time.

The requirements are shown in Table 1; they apply only under clear conditions.

Units: Ice age: Class
Ice edge motion: km/day

Table 1. Specifications of the VIIRS Sea Ice Age and Sea Ice Edge Motion EDR

Para. No.		Thresholds	Objectives	Specification Value
V40.7.8-1	a. Horizontal Cell Size (both Ice Age and Sea Ice Edge Motion)	3 km	0.1 km	2.4 km
V40.7.8-2	b. Horizontal Reporting Interval	(TBD)	(TBD)	Horizontal Cell Size
V40.7.8-3	c. Horizontal Coverage	Oceans	Oceans	N of 36 deg north latitude, S of 50 deg south latitude
	d. Measurement Range			
V40.7.8-4	1. Ice Age Classes	First Year, Multi-year (TBR)	New, Young, First Year, and Old (TBR)	New/Young, First Year, Multi-year *
V40.7.8-5	2. Ice Motion	0 – 50 km/day	0 – 50 km/day	0 – 50 km/day
V40.7.8-6	e. Probability of Correct Typing (Ice Age)	70 %	90 %	80 % (First Year versus Multi-year) 70 % (New/Young versus First Year
V40.7.8-7	f. Measurement Uncertainty (Ice Motion)	1 km/day	0.1 km/day	0.8 km/day
V40.7.8-8	g. Mapping Uncertainty	3 km	1 km	233 m (worst case)
V40.7.8-9	j. Minimum Swath Width	3000 km (TBR)	3000 km (TBR)	3000 km

* We use the term Multi-year ice throughout this document, but assume that it includes all types of ice surviving at least one season of melting

2.2 HERITAGE

2.2.1 Sea Ice Age

2.2.1.1 Passive Microwave

The classification of sea ice age from passive microwave brightness temperatures is well-established (Eppler *et al.*, 1992), and currently forms the basis for global ice age retrieval at various ice centers (Boardman *et al.*, 1995; Partington and Steffen, 1998).

A uniform slab of clear ice will emit microwave radiation proportional to its thickness. In sea ice, there can be many air bubbles and brine pockets that are unevenly distributed throughout the ice. The bubbles lower the emissivity, resulting in brightness temperature variations (Hall *et al*,

1981). Surface features, produced by freeze/thaw events and motion-driven collisions, will also modify the microwave signal (Eppler *et al*, 1992),. The same features affect surface reflectance, suggesting that there should be correlations between microwave and reflectance signatures of sea ice.

2.2.1.2 Synthetic Aperture Radar

Synthetic aperture radar (SAR) observations of sea ice have shown that radar backscatter signatures are characteristic of ice type, and can be used for classifying sea ice cover by imagery analysis (Jeffries, *et al*., 1994; Hall, *et al*., 1994). RADARSAT observations are being incorporated into the ice typing retrievals at ice centers. SAR-based retrievals have the advantage of good spatial resolution and allows coverage under cloudy conditions. Disadvantages are the limited aerial coverage and the lack of reliable automated classification algorithms. An additional disadvantage from an operational standpoint is the lack of contemporaneous data, since RADARSAT is on a separate platform.

2.2.1.3 AVHRR

The classification of sea ice age from visible-infrared data alone is difficult. Thick First Year ice is similar to Multi-year ice in its reflectance properties. Also, most sea ice surfaces will be snow covered. As a result, the use of measured reflectance to classify ice age types on a global basis has not been established, though some regionally based classifications have been made, using AVHRR channel 2. (Massom and Comiso, 1994).

Older ice tends to be colder in the winter, allowing for age typing derived from surface temperature, as derived from AVHRR channel 4 (Massom and Comiso, 1994).

An alternative approach shows promise. Yu and Rothrock (1996) and Lindsay and Rothrock (1993) have incorporated albedo and temperature data from AVHRR into an energy balance model to derive the thickness of the ice, with a reported accuracy of 50%.

Regional and seasonal ice conditions can be used in energy balance models along with observed temperature to infer age type. The incorporation of air temperature and snow depth as ancillary data will improve the accuracy of a classification of ice type using an energy balance model. The energy balance method has been incorporated into our ice age algorithm, as discussed in Section 3.3.2.2.

2.2.2 Sea Ice Edge Motion

The location of the sea ice edge is determined by ice drift in the marginal ice zones, and also by freezing and melting. The topology of the ice edge depends on the horizontal spatial scale used to report ice concentration. At small spatial scales, the topology will be complex due to the distribution of ice floes that typify the marginal ice zone. At greater spatial scales, the ice edge can usually be treated as a simple perimeter.

2.2.2.1 *In situ* (IABP / Argos)

The International Arctic Buoy program (IABP) has deployed hundreds of platforms which drift with the ice pack. The Argos system, utilizing NOAA satellites to position and to relay data from

the buoys, can determine drift motions with an accuracy better than 1 km/day (Thorndike, 1986). While accurate and reliable, these data are limited to the specific location of the buoys. They can be useful as a component in an ice motion product generated by data assimilation, and as a validation source for ice motion retrievals from remote sensing.

2.2.2.2 Passive Microwave (SMMR, SSM/I)

Passive microwave observations of sea ice motion have proven to be a valuable contribution to the study of polar regions (Eppler *et al*., 1992). Sea ice edge motion is required for the NPOESS/CMIS passive microwave sensor. The potential exists for a beneficial fusion of VIIRS and CMIS data, as discussed in Section 3.3.2.3 of this document. Ice motion from passive microwave remote sensing has the great advantage of global coverage under clear or cloudy conditions. The relatively coarse spatial resolution (> 10 km) is a drawback to the use of passive microwave data for ice motion in the marginal ice zone.

2.2.2.3 Synthetic Aperture Radar (RADARSAT)

Complex topologies have the advantage of facilitating ice motion analysis by tracking individual features in the ice pack. This technique is routinely applied to synthetic aperture radar imagery at operational ice centers. Most of this analysis is not automated. Automated algorithms to track ice motion are under development, but have not been established as operationally reliable. The current VIIRS algorithm will not rely on SAR imagery analysis for a retrieval, but will use it when available for validation. Future algorithm development may have the option of assimilating SAR results, under conditions to be determined.

SAR retrievals have the advantage of high spatial resolution and coverage under clear or cloudy conditions, but are too limited in swath for global operational needs.

2.2.2.4 Scatterometer (NSCAT)

Ice features can be identified by scatterometers, because surface roughness is a persistent characteristic of ice features. Liu, Zhao, and Wu (1999) have used NSCAT data, combined with data from the passive microwave SSM/I sensor, to obtain daily sea ice drift information in the Arctic. Scatterometer data provides an excellent complement to passive microwave data, since they observe independent properties of the same ice structures. As with passive microwave sensors, the relatively coarse spatial resolution of scatterometers limits their usefulness in mapping the MIZ.

2.2.2.5 Visible-Infrared (AVHRR)

At the VIIRS spatial scale, ice edge topology will be of intermediate complexity. Ice floes in the marginal ice zone (MIZ) will be identifiable, allowing us to identify ice distribution patterns that persist on a time scale of hours to days. In that case, we can use a maximum cross-correlation of "features" in successive ice images (Ninnis *et al*., 1986). This method has been used to determine ice motion from AVHRR data, with reported accuracies better than 1 km/day (Emery *et al*, 1991).

Retrieval of ice motion from visible-infrared remote sensing has been hampered by the inability of the sensor to observe the surface through cloud cover. Since the probability of cloud cover in

polar regions is high, the practical use of visible-infrared sensors has been discounted. There is, however, reason to believe that VIIRS will provide a valuable contribution to ice motion retrieval in the MIZ. An effective operational cloud mask, combined with an algorithm which can operate with masked images, can in principle result in a reliable Vis-IR ice motion retrieval.

The VIIRS sensor will be aboard three NPOESS platforms, resulting in 42 VIIRS orbits per day. At latitudes greater than 60 degrees, a given area will be monitored by VIIRS at least six times per day. This extended coverage should greatly improve the chances of finding a VIIRS image pair with a sufficient amount of clear area to allow MCC derivation of motion vectors.

2.3 INSTRUMENT CHARACTERISTICS

The VIIRS sensor is being designed based on the NPOESS sensor requirements and EDR thresholds and objectives. The Sea Ice Age algorithm uses ice reflectance and ice temperature derived by the ice concentration algorithm, as described in the VIIRS Imagery *[Y2466]* and Fresh Water Ice *[Y2404]* ATBDs. The ice concentration algorithm uses the VIIRS surface temperature Intermediate Product (IP) *[Y2405]* and the VIIRS Surface Reflectance IP in imagery bands. The characteristics of the VIIRS bands used to produce these products are shown in Tables 2 and 3.

Table 2. Sea Ice Age EDR – Input Data Summary (Spatial)

λ(μm)	Δλ(μm)	GSD (m) at Nadir (Track x Scan)	HSR (m) at Nadir (Track x Scan)	GSD (m) at Edge of Scan (Track x Scan)	HSR (m) at Edge of Scan (Track x Scan)
0.645	0.050	371 x 131	371 x 393	800 x 800	800 x 800
0.865	0.039	371 x 131	371 x 393	800 x 800	800 x 800
10.76	1.0	742 x 262	742 x 742	1600 x 1600	1600 x 1600
11.45	1.9	371 x 131	371 x 393	800 x 800	800 x 800
12.01	0.95	742 x 262	742 x 742	1600 x 1600	1600 x 1600

Table 3. Sea Ice Age EDR – Input Data Summary (Radiometric)

λ(μm)	Δ λ(μm)	Ltyp (W/m2-sr-um) or Ttyp	SNR / NEdT at Nadir	SNR / NEdT at Edge of Scan
0.645	0.050	22.0	317.9	183.5
0.865	0.039	25.0	418.7	241.7
11.45	1.9	210 K	0.43 K	0.74 K

The Sea Ice Edge Motion algorithm relies on ice concentration maps and ice edge boundary contours produced as part of the VIIRS Imagery EDR *[Y2466]*. There is no other specific demand on the VIIRS sensors.

Additional details on the instrument design are provided in the Raytheon VIIRS Sensor Specification document *[PS 154640-001]*.

2.4 RETRIEVAL STRATEGY

2.4.1 Sea Ice Age

The VIIRS Sea Ice Age algorithm classifies each VIIRS pixel as open water, New/Young ice, First Year ice, or Multi-year ice.

The input data will consist of a 2-dimensional grid of geo-located ice surface reflectance and geo-located ice surface temperature, produced by the ice concentration algorithm *[Y2466]*. The input data will contain a cloud mask tag from the VIIRS Cloud Mask *[Y2412]*. Each pixel with ice concentration greater than zero will be processed for ice type classification. New/Young or First Year/Multi-year ice will be classified from reflectance during daytime or from temperature during nighttime. Pixels classified as First Year/Multi-year will be further processed to be classified as First Year or Multi-year.

2.4.2 Sea Ice Edge Motion

The VIIRS Sea Ice Edge Motion algorithm derives a motion vector for each horizontal cell that contains an ice edge.

The input data will include the current VIIRS ice concentration image, produced by the ice concentration algorithm as part of the Imagery EDR *[Y2466]*. The most recent ice concentration image will be acquired from an external ice concentration store. This store will be populated by VIIRS ice concentration retrievals, and will be maintained by the VIIRS system. The input data will also include the current VIIRS ice edge location coordinates, produced by the ice edge location algorithm as part of the Imagery EDR *[Y2466]*.

3.0 ALGORITHM DESCRIPTION

3.1 PROCESSING OUTLINE

3.1.1 Sea Ice Age

The VIIRS Sea Ice Age algorithm is retrieved from an integrated software process that produces all of the VIIRS Ice EDRs. A description of the software process flow is in the VIIRS Snow/Ice Module Software Architecture document *[Y2477*].

The VIIRS Sea Ice Age algorithm uses three different methods:

(1) Nighttime discrimination of New/Young ice from thicker First Year and Multi-year ice is achieved by an energy balance derivation of ice thickness from ice temperature. Surface air temperature and snow depth are required ancillary data for this method. Surface air temperature will be acquired from recent CMIS temperature profile retrievals (c.f. Section 4.2.1.2). Snow depth will be acquired from climatology (c.f. Section 3.3.2.1). Details of this approach are in Section 3.3.2.1.

(2) Daytime discrimination of New/Young ice from thicker First Year and Multi-year ice is achieved by application of a reflectance threshold. Details of this approach are in Section 3.3.2.2.

(3) Multi-year ice is distinguished from First Year ice by a filtered distribution of ice reflectance (daytime) or ice temperature (nighttime). Details of this approach are in Section 3.3.2.3.

All three methods use reflectance and temperature corresponding to ice itself, corrected according to ice fraction retrieved by the automated ice concentration algorithm described in the Imagery ATBD *[Y2466]*.

The process selects either the reflectance-based algorithm or the temperature-based algorithm, depending upon solar zenith angle and surface air temperature to make a decision.

New or Young ice pixels are identified by method (1) or method (2).

The remaining ice pixels are passed to the algorithm which implements method (3) to identify a pixel as First Year or Multi-year. This algorithm uses the most recent local ice age spatial distribution to help make the classification.

3.1.2 Sea Ice Edge Motion

The VIIRS Sea Ice Edge Motion algorithm is retrieved from an integrated software process that produces all of the VIIRS Ice EDRs. A description of the software process flow is in the VIIRS Snow/Ice Module Software Architecture document *[Y2477*].

VIIRS data from the current orbit are used to derive ice concentration *[Y2466]*. The current ice concentration image and the most recent suitable ice concentration image are selected as an image pair for the MCC analysis. Application of the MCC to these image pairs produces ice motion vectors.

The ice edge location is derived from the ice concentration by a separate algorithm *[Y2466]*, and used to interpolate the ice motion vectors to the ice edge location, resulting in ice edge motion vectors.

The algorithm derives ice edge motion through the following steps:

(1) Maximum Cross Correlation is applied to a sequential pair of ice concentration images to derive motion vectors

(2) Nearest neighbor filtering is applied to remove "bad" vectors

(3) The image is gridded to a horizontal cell size. Each horizontal cell is searched for the presence of at least one ice edge pixel.

(4) The ice edge location of each edge cell is computed from all edge pixels in the cell

(5) The ice edge motion vector is computed by a weighted interpolation of the motion vectors derived by steps (1) and (2).

3.2 ALGORITHM INPUT

3.2.1 VIIRS Data

The ice age algorithm requires the VIIRS data listed in Table 4. The ice edge motion algorithm requires the VIIRS data listed in Table 5.

Table 4. VIIRS Data for the Sea Ice Age Algorithm.

Input Data	Source of Data	Reference
Instrument Quality	VIIRS RDR to SDR Conversion	*[Y3261]*
Solar / Sensor Geometry	VIIRS RDR to SDR Conversion	*[Y3261]*
Cloud Mask	VIIRS Cloud Mask Algorithm	*[Y2412]*
Ice Surface Reflectance	VIIRS Imagery Algorithm	*[Y2466]*
Ice Surface Temperature	VIIRS Imagery Algorithm	*[Y2466]*
Ice Age Spatial Distribution	VIIRS Ice Age Spatial Distribution Store	*[Y2466]*
Snow Depth	VIIRS LUT	*This document*

Table 5. VIIRS Data for the Sea Ice Edge Motion Algorithm.

Input Data	Source of Data	Reference
Instrument Quality	VIIRS RDR to SDR Conversion	*[Y3261]*
Geo-location	VIIRS Earth Location Algorithm	*[Y3258]*
Solar Geometry	VIIRS RDR to SDR Conversion	*[Y3261]*
Cloud Mask	VIIRS Cloud Mask Algorithm	*[Y2412]*
Current Ice Concentration	VIIRS Imagery Algorithm	*[Y2466]*
Previous Ice Concentration	VIIRS Ice Concentration Store	*[Y2466]*
Current Ice Edge Location	VIIRS Imagery Algorithm	*[Y2466]*

3.2.1.1 Instrument quality

Each pixel should have a quality flag. Pixels with instrument quality below a threshold, to be determined, shall be excluded from further processing. Instrument quality flags will be set by the Build-RDR processor.

3.2.1.2 Solar Geometry

Pixels with solar zenith angle greater than a threshold shall have ice age retrieved from temperature data. Pixels with solar zenith angle smaller than a threshold, shall have ice age retrieved from reflectance data. The setting of these thresholds will be part of initialization (c.f. Section 4.4.1). It is expected that there will be a transition range over which the reflectance-based result is progressively de-weighted to produce a seamless day/night transition.

3.2.1.3 Cloud Mask

An effective, reliable cloud mask is essential to the successful performance of automated sea ice retrievals from Visible-Infrared remote sensing data..

The VIIRS Cloud Mask IP *[Y2412]*, building on MODIS heritage (Ackerman *et al*., 1997), is expected to derive for each pixel a status of clear/cloudy, following the convention of the MODIS cloud mask. Pixels flagged as definitely cloudy will be excluded from further processing. We expect that pixels flagged as probably cloudy will also be excluded, though this determination must depend on an assessment of the cloud mask performance, particularly over snow and ice surfaces. Pixels flagged as probably clear will be processed, though we may wish to flag the output EDR as possibly cloud contaminated. Pixels flagged as definitely clear will be processed.

It is anticipated that the cloud mask will also flag pixels that are shadowed by clouds. It is expected that these pixels will be excluded from further processing, though we may wish to conduct testing to determine what the threshold for cloud shadowing should be. Ice edges are often associated with clouds, increasing the critical need for effective cloud masking for ice edge motion.

3.2.1.4 Ice Surface Reflectance

Ice surface reflectance is derived from the Surface Reflectance IP *[Y2411]* by the ice concentration algorithm *[Y2466]*, and used to classify ice age during daytime.

3.2.1.5 Ice Surface Temperature

Ice surface temperature is derived from the Surface Temperature IP *[Y2405]* by the ice concentration algorithm *[Y2466]*, and used to classify ice age during nighttime.

3.2.1.6 VIIRS Ice Age Spatial Distribution

The most recent local spatial distribution of ice age classes is used to help classify ice as First Year or Multi-year (c.f. Section 3.3.2.3). The algorithm acquires this information from a stored database. This store will be populated by VIIRS ice age retrievals and by CMIS ice age retrievals, and will be maintained by the VIIRS system.

3.2.1.7 Snow Depth

Ice age classification from energy balance (c.f. Section 3.3.2.1) requires information on snow depth. The snow depth will be acquired from a look up table, which will contain the ratio of snow depth to ice thickness for a given region and season. This LUT will be created from climatological histories of snowfall rate and air temperature, as explained in Section 3.3.2.1.

3.2.1.8 Geo-location

Geo-location is required for ice edge location, from which we derive ice edge motion. Geo-location errors, obtained from the Raytheon VIIRS System Specification, are used in our performance analysis (Section 4.2.2).

3.2.1.9 Current Ice Concentration

The ice concentration map for the current VIIRS orbit, derived by the Imagery algorithm *[Y2466]*, is one member of the image pair used to derive ice motion.

3.2.1.10 Previous Ice Concentration

The ice concentration map from the most recent previous VIIRS orbit, is the other member of the image pair used to derive ice motion. It is acquired from the VIIRS ice concentration store, where it was placed by the Imagery algorithm *[Y2466]* during the previous orbit.

3.2.1.11 Current Ice Edge Location

The coordinates of the ice edge are derived by the Imagery algorithm *[Y2466]*, and used to interpolate the ice motion vectors to the ice edge location, thus producing the ice edge motion vectors.

3.2.2 Non-VIIRS data

The required Non-VIIRS data for the Sea Ice Age EDR is summarized in Table 6.

Table 6. Ancillary Non-VIIRS data for the Sea Ice Age/Edge Motion EDR

Input Data	Source of Data
Ice Age Spatial Distribution	NPOESS / CMIS
Surface Air Temperature	NPOESS / CMIS

3.2.2.1 CMIS Ice Age Spatial Distribution

The most recent local spatial distribution of ice age classes is used to help classify ice as First Year or Multi-year (c.f. Section 3.3.2.3). The algorithm acquires this information from a store. This store will be populated by VIIRS ice age retrievals and by CMIS ice age retrievals, and will be maintained by the VIIRS system.

3.2.2.2 Surface Air Temperature

The ice age nighttime algorithm requires recent surface air temperature to calculate the heat flux through the ice sheet, as discussed in Section 3.3.2.1.

Air temperature can be determined by NPOESS/CMIS. It will be desirable for CMIS to report surface air temperature, though it is not a specified SRD requirement for either sensor. At polar latitudes, we expect to obtain 4 CMIS samplings of a given location per day. We will use the latest two observations, with an expected error of 0.6 K, as discussed in Section 4.2.1.2.

3.3 THEORETICAL DESCRIPTION OF THE RETRIEVAL

In the following sections, the mathematical background of the processes outlined in Section 3.1 will be described. These processes only apply to regions that successfully passed the quality examinations.

3.3.1 Physics of the problem

Ice age and concentration are derived from the differences in reflectance and temperature characteristic of ice in various stages of development. The characteristics of ice surfaces are influenced by their accumulated snow cover. An understanding of the effect of snow on the surface reflectance and surface temperature is required.

3.3.1.1 Snow reflectance

Pure snow is a distinctive target across a part of the solar spectrum. It is among the brightest of natural substances in the visible and near-infrared part of the spectrum, but it is also often the darkest in the shortwave infrared (Dozier, 1989). The reflectance of snow depends on wavelength, and this dependency is controlled by the imaginary part *(k)* of the complex refractive index. This reaches a minimum at a wavelength of about 0.46 microns, and increases by a factor of 10^6 - 10^7 as wavelength increases out to 2.5 microns (Warren, 1982; Dozier, 1989). Light transmission decays exponentially in snow across a distance *d* as $\exp(-4\pi kd/\lambda)$. The *e*-

folding distance for snow (the distance over which transmittance is reduced to 1/e) decreases from more than 20 m in the 0.4 – 0.5 micron range to less than 1 mm at 1.6 microns.

Light in snow is scattered primarily by refraction through, not reflection from, the ice grains. Photons are scattered at the grain surfaces, but absorbed while traversing the grain interiors. Only about 3 percent of the light scattered by an ice grain is reflected from the external surface. Nearly 89 percent is refracted through the grain, and 8 percent is scattered after internal reflections (Bohren and Barkstrom, 1974). Because ice is so transparent to visible radiation, snow reflectance is insensitive to grain size in bands below 0.7 microns, but sensitive to absorbing impurities in the snow (Wiscombe and Warren, 1980; Grenfell *et al.,* 1981). Because absorption by ice is much stronger in bands above 1.4 microns, reflectance at these wavelengths is insensitive to absorbing impurities, but sensitive to grain size. Absorbing particulates affect snow reflectance out to 0.9 microns (Grenfell *et al.,* 1981; Warren and Wiscombe, 1980), so the 0.86 micron band is sensitive to both absorbing impurities and grain size. All aforementioned values in this paragraph are determined from geometric optics for a sphere.

The spectral signature of snow is unique among common substances. Clouds and snow are both bright across the visible and near-infrared region, but clouds are much brighter than snow in the shortwave infrared. This is because the smaller size of the scatterers in clouds decreases the probability of absorption in this spectral region where ice and water are moderately absorptive (Crane and Anderson, 1984; Dozier, 1984, 1989). Conversely, bodies of open water are dark at all wavelengths.

The physical basis of snow reflectance is also discussed in the VIIRS Snow Cover/Depth ATBD *[Y2401]*.

3.3.1.2 Ice Reflectance

Reflectance from ice surfaces differs from snow reflectance because the ice consists of sheets rather than grains. Clear ice slabs are highly transmitting (Bolsenga, 1983). Reflectance occurs by scattering from impurities, such as brine pockets and air bubbles. Therefore, the reflectance observed from natural ice surfaces is highly variable, depending on the condition of impurities for a given ice sheet. Given the wide variety of ice conditions in nature, ice reflectance is not as well determined as snow reflectance, which is amenable to Mie scattering theory (Warren, 1982) Studies of ice reflectance thus tend to be empirical.

Remote sensing studies of sea ice are relatively widespread and are of significant potential benefits. The wide range in spectral reflectance observed in sea ice of various types and thickness is a well-established characteristic of sea ice. This characteristic is an important factor in the reflectance-based retrieval of ice age for new, young and First Year sea ice.

Spectral reflectanceof sea ice at various bands undergoes significant changes depending upon ice structure and the condition of the ice surface. Spectral reflectance curves differ for different ice age. Each ice age has its own unique spectral signature, as shown in Table 7.

Table 7. Reflectance Characteristics of Ice Age Types

Stage of ice development	Characteristic thickness	Ice color	International nomenclature	SRD classes	Our interpretation of

						classes
Initial ice crystals	Less than 5 cm	Dark, mat	New ice	New Ice		New ice
Mat thin elastic ice	Up to 10 cm	Mat, whitish	Nilas			
Gray bending stable ice	10 – 30 cm	Grey, grey-white	Young ice	Young ice		Young ice
White fracturing ice of First Year grow period	More than 30 cm	White, light green, Greenish	First Year ice	First Year ice		First Year ice
Ice in the second year cycle of development	N/A	Green-blue	Second-Year ice		Old ice	Multi-year ice
Ice surviving more that two year cycles	N/A	Blue	Multi-Year ice	M-y ice		

On the whole, ice reflectance is correlated with ice age as it varies during the seasonal cycle.

The correlation of snow depth with stage of development also contributes to the characteristic reflectance signature of different ice age classes.

3.3.1.3 Water Reflectance

The reflectance spectral signature of open water is significantly different from snow/ice reflectance, except for the thinnest ice surfaces. This reflectance contrast allows for a calculation of ice fraction during daytime by the derivation of distinct ice and water reflectance tie points. The algorithm for retrieval of ice concentration *[Y2466, Y2405]* derives the tie points. The ice reflectance tie points are passed to the ice age daytime algorithm.

3.3.1.4 Surface Temperature

During a great part of the seasonal cycle, infrared bands will be the only available information to retrieve ice age and ice fraction. Infrared radiance allows us to calculate surface temperature. Infrared information is useful when there are thermal contrasts between water and ice surfaces.

Changes in sea ice surface temperature are governed by the joint influence of vertical heat fluxes of different origin. The intensity of turbulent exchange by heat between the atmosphere and underlying ice surface, as well as the surface balance of long-wave radiation, directly depend on ice surface temperature. Vertical heat flux through ice cover is an explicit function of the vertical ice temperature profile, which depends on ice surface temperature. Thus, all main components of heat exchange between the atmosphere and the underlying ice surface (except short-wave radiation fluxes) are explicit functions of ice surface temperature.

In the winter, heat flux between the atmosphere and ice is compensated by ice growth at the underside of the ice. There are no vertical changes in heat flux at the boundary between air and ice surface. At the same time, many components of heat flux depend on ice surface temperature. Therefore, conditions of conservation of vertical heat flux at the surface can be fulfilled only if ice surface temperature is adjusted to varying influencing environmental conditions.

Ice thickness is the main factor determining vertical heat flux through the ice under specified atmospheric conditions. Thus, a general conclusion about the relation between ice surface temperature and thermodynamic processes in ice cover and atmospheric boundary layer can be formulated. Ice surface temperature is determined by the processes of vertical heat exchange and is a distinctive indicator of ice thickness. Given the same atmospheric conditions, New or Young ice will have a lower surface temperature than thicker First Year ice.

3.3.1.5 Sea Ice Edge Motion

Sea ice edge motion, defined as a displacement of a sea ice edge, is a product derived from the motion of sea ice concentration features in the vicinity of an ice edge. Ice moves in response to surface wind, ocean currents, and stresses from neighboring ice. Ice motion can be translational, rotational, or deformational. Deformational motion is not a great factor in the MIZ, where individual floes tend to be separated by open water. Rotational motion is important on large spatial scales, where the ocean circulation patterns become evident. Our retrievals will occur on smaller spatial scales, where translational motion is expected to dominate.

The tracking of ice features by correlation methods has been shown to work well for translational motions (Agnew et al., 1997; Kwok et al., 1998).

3.3.2 Mathematical description of the Sea Ice Age algorithm

Our algorithm classifies ice type by using three methods:

(1) Nighttime discrimination of New/Young ice from thicker First Year and Multi-year ice is achieved by an energy balance derivation of ice thickness from ice temperature. Nighttime is determined by a solar zenith angle threshold.

(2) Daytime discrimination of New/Young ice from thicker First Year and Multi-year ice is achieved by application of a reflectance threshold. Daytime is determined by a solar zenith angle threshold.

(3) Multi-year ice is distinguished from First Year ice by a filtered distribution of ice reflectance (daytime) or ice temperature (nighttime). The transition from daytime to nighttime is determined by a solar zenith angle threshold.

All three methods use reflectance and surface temperature corresponding to ice itself, corrected according to ice fraction retrieved by automated algorithm described in Imagery ATBD *[Y2466]*.

Our performance analysis (c.f. Section 4.2.1) is based on the visible reflectance and surface temperature only. In principle, the use of NIR reflectance can improve daytime performance, provided that the visible and NIR bands are properly weighted. The relative weight of visible and NIR reflectance will be determined by pre-launch verification (c.f. Section 4.4).

3.3.2.1 Energy Balance Model

We use data on ice surface temperature and surface air temperature to calculate ice thickness (age) on the basis of a thermodynamic model of energy balance. Parameters of the thermodynamic model are determined as functions of season and region. Regional studies

demonstrate that such calculations can effectively discriminate ice age for a range of sea ice age from new ice through medium First Year ice (Yu and Rothrock, 1996).

The equation of heat balance is usually used as a basis for calculating thermodynamic changes of sea ice mass. The equation includes the heat fluxes of different origination: radiation, turbulent fluxes, ice heat conductivity. If information on air temperature and ice surface temperature is available, we can transform the mathematical formulation and use the same equation of heat balance to determine ice thickness (age).

In the summer there is no significant contrast between surface temperature for different ice type or even open water. Retrieval from thermal bands may not meet our specification under these conditions. Therefore, the main attention will be devoted to consideration of thermal processes in the winter.

The equation of surface heat balance for ice (snow) surface reflects the conservation of vertical heat flux. In other words, heat flux between ice surface and the atmosphere is equal to resultant heat flux through ice.

In general, the equation of surface heat balance has the following form:

$$Q_s = Q_\Sigma(1-\alpha) + E_a - E_s + Q_t + Q_e, \qquad (3.3\text{-}1)$$

where Q_S - resultant heat flux from the ice (snow) surface to the atmosphere,

Q_Σ - total incident short-wave solar radiation,

α - surface albedo,

E_a - long-wave radiation from the atmosphere,

E_S - long-wave radiation from surface,

Q_t - turbulent heat exchange,

Q_e - heat exchange due to evaporation.

Total incident shortwave solar radiation is a sum of direct solar radiation projected onto a horizontal surface and diffusive radiation. It depends upon solar zenith angle, latitude, day of seasonal cycle, atmosphere transparency, and cloudiness. We do not partition total short-wave solar radiation into direct and scattered radiation as their combined effect is important for energy calculation.

The absorbed fraction of solar radiation depends upon the state of ice (snow) surface. The surface reflectance varies in a very wide range, from a few percent for water surface up to 98% for fresh snow. Albedo is a very important factor determining variability of the surface heat balance.

The second and the third terms of Equation 3.3-1 determine fluxes of long-wave radiation. Different mathematical forms were proposed by researchers to present these terms in the equation. Existing empirical formulae reflect dependence of the fluxes on air temperature, humidity, and cloudiness. As an appropriate approximation, we can use magnitudes of air temperature and humidity near the surface (2 m above surface is a standard height).

We propose to use the results of radiation balance studies in the polar areas to calculate long-wave heat fluxes near the surface. Magnitudes of air temperature and humidity at the level of 2 m are considered to be sufficient to calculate long-wave radiation from the atmosphere. We chose the following formula obtained on the basis of processing numerous measurements of radiation fluxes:

$$E_a = (a + b \sqrt{e}\,)\,(1 + c\,E)\,\sigma_B\,T_a^4, \qquad (3.3\text{-}2)$$

where σ_B - Stephan-Boltzmann constant,
T_a - Air temperature
e - absolute air humidity
E - cloud fraction

Empirical coefficients a, b, and c characterize regional conditions in high latitudes. The first expression between the brackets describes influence of humidity. The humidity exerts a significant effect on variation of long-wave radiation from the atmosphere in low and moderate latitudes. In the polar regions, the effect of humidity is less noticeable. The second expression in the brackets accounts for the influence of clouds.

Long-wave radiation flux from a surface is determined as:

$$E_s = \mu\,\sigma_B\,T_s^4 \qquad (3.3\text{-}3)$$

where μ - surface emissivity
T_s - surface temperature

The two last terms in Equation 3.3-1 reflect the influence of turbulent heat exchange. We propose to use the simple bulk formulae defining the turbulent fluxes as proportional to difference between air temperature and specific humidity (g) at two levels:

$$Q_t = K_t\,(T_a - T_s) \qquad (3.3\text{-}4)$$

$$Q_e = K_e\,(g_a - g_s) \qquad (3.3\text{-}5)$$

where K_t, K_e - coefficients of proportionality
g_a – specific humidity of air at 2 meters
g_s – specific humidity of saturation at ice surface

These simple formulae can give us reliable results of determining turbulent fluxes only in the case when the coefficients of proportionality are defined as functions of influencing factors.

We assume the following form for K_t and K_e:

$$K_t = \rho_a\,C_a\,C_t\,V \qquad (3.3\text{-}6)$$

$$K_e = \rho_a\,L_a\,C_e\,V \qquad (3.3\text{-}7)$$

where ρ_a – air density
C_a – specific heat
L_a – latent heat of evaporation
V - wind velocity
C_t, C_e - dimensionless coefficients of proportionality

C_t and C_e are equal but depend upon atmospheric stratification. The magnitudes of these coefficients are approximately the same for unstable stratification in the lower levels of the atmosphere and for neutral stratification. For average conditions in polar regions, the magnitude of the dimensionless coefficients is 0.0017.

The resultant heat flux from the ice (snow) surface to the atmosphere can be determined as:

$$Q_s = \lambda \frac{\partial T}{\partial Z} \tag{3.3-8}$$

where λ is thermal conductivity.

The heat flux through ice cover depends on ice thickness. This circumstance allows us to calculate ice thickness, assuming that the other components of the heat exchange between the atmosphere and underlying surface are known or can be approximated.

We intend to use the algorithm to calculate the thickness of new, young, and First Year ice types. For these types, the ice is sufficiently thin to allow a linear approximation of the vertical ice temperature profile. In that case, the heat flux through ice cover can be determining on the basis of the following approximation of Equation 3.3-8:

$$Q_s = \lambda_i \frac{T_s - \theta}{H} \tag{3.3-9}$$

where λ_i - thermal conductivity of ice
θ - freezing temperature of water
H - ice thickness.

The thermal conductivity of snow differs from ice. If ice is covered by snow, we must modify Equation 3.3-9 to account for the heat flux through the snow cover:

$$Q_s = \frac{T_s - \theta}{\frac{h}{\lambda_s} + \frac{H}{\lambda_i}} \tag{3.3-10}$$

where h - snow depth,
λ_s - thermal conductivity of snow.

If we assume that all components in the right side of the Equation 3.3-1 are known, we can replace the left side of Equation 3.3-1 with 3.3-9 or 3.3-10, and express the ice thickness as:

$$H = \frac{\lambda_i (T_s - \theta)}{Q_\Sigma (1-\alpha) + E_a - E_s + Q_t + Q_e} \tag{3.3-11}$$

or, when there is snow cover:

$$H = \frac{\lambda_i (T_s - \theta)}{Q_\Sigma (1-\alpha) + E_a - E_s + Q_t + Q_e} - \frac{\lambda_i h}{\lambda_s} \tag{3.3-12}$$

The algorithm will acquire snow depth (h) as a fraction of ice thickness (H) from a regional, seasonal LUT, which will be created by combining characteristic rates for ice growth and snowfall.

We propose to develop LUTs that are to be used to transform calculated ice thickness into ice age.

3.3.2.2 Reflectance Threshold Method

The energy balance method does not perform as well during daytime, because the short-wave radiation flux error is too large. An alternative method is needed to retrieve classification of first year ice types during daytime. Our approach is to apply reflectance thresholds.

Stage of ice development (ice age) can be considered as a thermodynamic characteristic of ice, reflecting its growth. One of the most prominent features of different stages of ice development is ice color. New ice is characterized by dark, mat, whitish color. Young ice is gray and gray-white. First Year and Multi-year ice has higher reflectance. New ice and nilas as well as gray ice have a wet surface. Snow cover does not accumulate on these types of ice and does not modify their reflectance. Snow cover can be observed on gray-white ice, but this type of young ice still has lower reflectance than thicker ice.

Thus, by definition, different stages of ice development are characterized by different reflectance. This allows one to use a straightforward threshold approach to distinguish new and young ice.

Different ice types exhibit different spectral reflectance. This difference in reflectances is used for discrimination between New/Yong and First Year/Multi-year ice types at daytime. Using the reflectance of visible and near-infrared bands is an effective and straightforward way to retrieve ice type for relatively thin ice cover.

This approach will complement the energy balance method, allowing us to meet Measurement Range objectives during daytime as well as night.

We recommend the development of regional (and seasonal) LUTS to transform retrieved ice surface reflectance into ice age.

3.3.2.3 Discrimination between First Year Ice and Multi-year Ice

Probability densities of ice parameters such as reflectance, albedo, temperature are overlapped for different ice types. Therefore, classification based on applying thresholds in many cases is unable to distinguish between First Year ice and Multi-year ice. Even mean values of parameters for these ice types vary in a significant range, depending on local conditions and season. The range of variability is approximately the same for Multi-year ice and relatively thick First Year ice. It means that any kind of predetermined thresholds or similar approaches could not be used. Published results (Grenfell and Maykut, 1977 ; Massom and Comiso, 1994; De Abreu et al., 1995) and our own estimate confirm the situation.

Automated classification algorithm needs to take into account image texture characteristics. In the very general sense, image texture can be defined as the frequency of spatial changes in parameter values in a local region under consideration. There are different possible quantitative measures of texture. The problem of classification of ice types is complicated by the fact that ice cover presents a mixture of different stages of its development (age). To calculate texture parameters for areas containing several ice types, we first need to classify image pixels.

Our approach to ice classification is based on using iterative procedures involving application of a spatial filter, identification of principal peaks in probability densities (corresponding to ice classes), and segmentation.

Spatial Filtering

There are numerous different kinds of filters. An optimal filter should suppress noise without destroying even fine features in image. VIIRS instruments are characterized by relatively low noise. Thus suppressing noise is a secondary function of filtering. Filtering plays mostly a supplementing role for the following segmentation.

The probability density of any specified parameter corresponds to the mixture of different ice types. The filter sharpens peaks and valleys of probability density. The repeated application of an optimal filter can transform an original unimodal probability density into a multimodal distribution (Lythe, Hauser, and Wendler, 1999; Lee and Jurkevich, 1989; Smith, Barret, and Scott, 1995). The process of averaging tends to cluster pixels together in the same class, moving pixels away from the valleys toward more pronounced peaks in probability densities.

We assume that clear peaks in probability density correspond to different ice classes. Approximate class boundaries are determined as the principal intermediate low points between the peaks. In many cases even after filtering, the placement of boundaries is not accurate as the valleys are not clearly defined. But the accurate placement of valleys is not required, as in the segmentation procedure the placement of peaks is the critical factor. It is the relative movement of a pixel value toward or away from a peak in response to filtering that determines the final class of ice, rather than the placement of the boundaries between peaks.

We need to apply filter that will preserve the main features of the image. We use the sigma filter, which replaces the central pixel in a search window by the average value of all window pixels within two standard deviations of the central pixel value (Lee, 1983).

The sigma filter is based on the fact that more than 95% of normally distributed samples fall within two standard deviations on either side of the mean value. Thus, the sigma filter excludes from averaging those values that correspond to different ice type.

We apply the simplest sigma filter within 3 x 3 moving window. The value of the central pixel is replaced by the average of the corresponding ice class if at least three pixels in the window belong to the same class.

We would like to emphasize that the procedure of filtering is incorporated in our algorithm to transform the histogram of ice characteristic (reflectance or temperature) to less noisy form. The resulting distribution of ice characteristic is much smoother, and at the same time the peaks and valleys in the distribution become more pronounced.

Segmentation

Segmentation can be considered as a mandatory phase of ice classification. Segmentation significantly improves classification accuracy. Segmentation identifies features of ice distribution and therefore can be also useful for detecting ice motion between two successive images.

Segmentation of an image is critically important to ice type classification. Any type of texture measure will be erroneous if the analyzed window includes a mixture of ice classes.

Segmentation allows us to distinguish different ice classes and calculate the texture parameters after separation of different classes. Thus, we avoid errors caused by joint analysis of unseparated ice classes.

There are quite different approaches to segmentation. We are sure that segmentation of ice classes should use spatial distribution of ice parameters in addition to analysis of their probability densities. Only using spatial distribution of ice parameter leads to retrieval of contiguous regions occupied by different ice classes.

In the segmentation stage after each application of the sigma filter, each pixel is examined to determine whether it converges to any peak in probability density. The pixel is considered to be converging to a peak application of the filter shifts its value away from a valley and toward the peak. A pixel is assumed to belong to the ice class corresponding to a peak if, in 3 x 3 window, at least two other pixels have already converged or are converging to the same peak. On the following iterations, filtering and segmentation is applied only to unconverged pixels.

At the second step of segmentation, we test two possible ice classes for all still unclassified pixels. One class has a mean parameter value larger than the value of the central pixel. The other class has a smaller mean value. If only one of neighboring ice types contains three or more pixels, the central pixel belongs to the same class. If both neighboring ice types contain at least three pixels, the central pixel belongs to the class characterized by the mean least displaced from the central pixel.

At the last step of segmentation, we classify those pixels that do not belong to ice class with at least three pixels in the window.

Segmentation of an image into ice classes significantly helps to remove ambiguity. Each ice class can then be characterized by the predominant value of the parameter instead of by overlapping probability densities.

Figure 1 illustrates the method, using an AVHRR visible band image of the Chukchi Sea in early September before onset of freezing. The figure shows the distribution of retrieved ice classes for the Chukchi Sea AVHRR scene after filtering and segmentation.

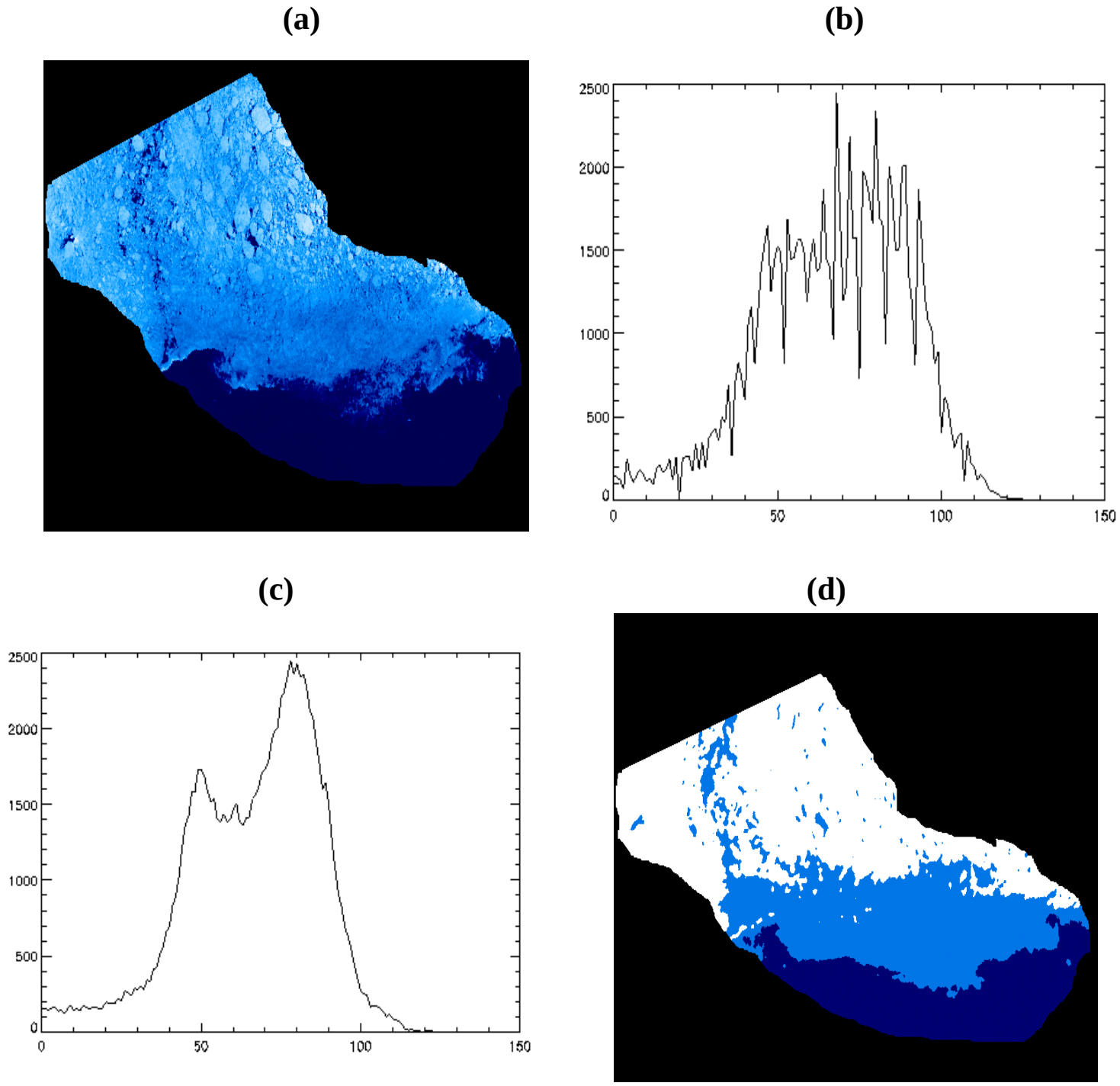

Figure 1. Visible image of ice cover in the Chukchi Sea (a). The distribution of ice reflectance before filtering (b) and after filtering (c). The classification of the scene after filtering and segmentation. Multi-Year ice is white, First-Year ice is light blue. Open water is dark blue.

Ice Types

Distinction between new ice, young ice, and following stages of ice development can be determined on the basis of any parameter depending on ice thickness: reflectance, albedo, or temperature.

Distinction between First Year ice and Multi-year ice is not easy. But the following different possible approaches can be used.

First, different stages of ice development are characterized by various quantitative measures of texture. A set of quantitative measures can be used as a look-up table to assign each ice class to a specified stage of ice development. The look-up table will be tested and developed during the next phase of the algorithm development.

Another approach to distinguish First Year ice from Multi-year ice is based on other potentially available sources of information on ice distribution. Multi-year ice could not become First Year ice and could not disappear if other types of ice present. On the other hand, First Year ice transforms into Multi-year ice only once during seasonal cycle, at the moment of water freezing. Thus, information on the presence of Multi-year ice in the area under consideration can enable us to distinguish First Year ant Multi-year ice. If Multi-year ice occurred in the area at the preceding time we will assign ice classes with the highest reflectance and lowest temperature in the wintertime to Multi-year ice.

We recommend using CMIS information on the stage of ice development or distribution of ice age obtained by VIIRS from previous satellite passes.

3.3.3 Mathematical description of the Sea Ice Edge Motion algorithm

Maximum Cross Correlation: MCC is a well-established technique for deriving the displacement of features in a sequential image pair. A template window is defined for one of the images (Image 1) and a larger search window is defined for the other image (Image 2). For a given pixel (i) in Image 1, the cross-correlation with a pixel (j) of Image 2 is computed as:

$$C = \frac{\sum_k \sum_m \left(P_2 (X_k - \delta X , Y_m - \delta Y) - \langle P_2 \rangle \right) \left(P_1 (X_k , Y_m) - \langle P_1 \rangle \right)}{\sum_k \sum_m \left(P_1 (X_k , Y_m) - \langle P_1 \rangle \right) \left(P_1 (X_k , Y_m) - \langle P_1 \rangle \right)} \qquad (3.3\text{-}13)$$

Where: P = value of the parameter to be correlated (e.g. temperature)
X = x-coordinate of image
Y = y-coordinate of image
k = range of x-coordinates in template window
m = range of y-coordinates in template window
δX = x-displacement of pixel (j) from pixel (i)
δY = y-displacement of pixel (j) from pixel (i)
<P> = mean value of the parameter in the template window

The range of δX and δY are determined by the size of the search window. For each value of (δX , δY) in the search window, a correlation C = C (δX , δY) is computed. The (δX , δY) with the largest C is selected. If its C value is greater than a threshold value, a displacement vector is defined with a start point at pixel (i) and an end point displaced by (δX , δY). The motion vectors are computed from the displacement as :

$$V_X = \delta X / \delta t \ , \quad V_Y = \delta Y / \delta t \qquad (3.3\text{-}14)$$

Where δt is the time interval between the image pairs.

The MCC process is illustrated in Figure 2.

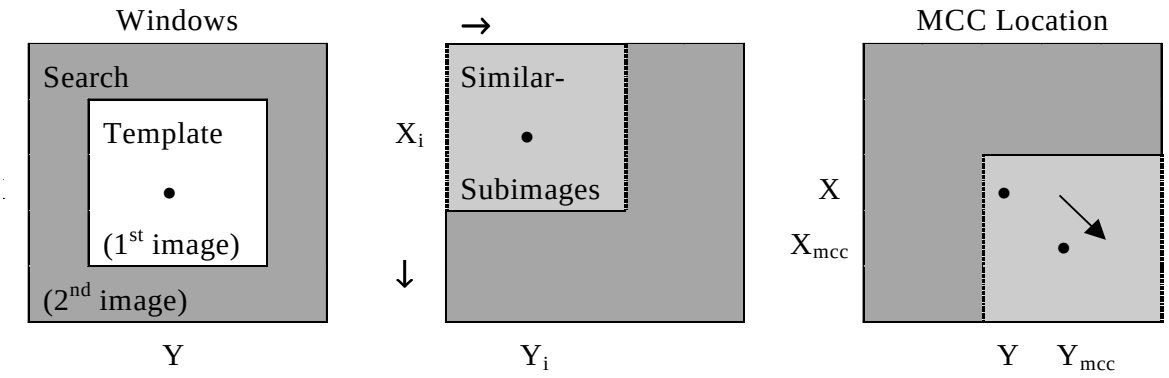

Figure 2. Illustration of the MCC process, Domingues (1999).

Filtering: Experience has shown that the set of displacement vectors derived by application of equation 3.3-13 will often contain "bad" vectors. These are caused by noise in the system. In Sources of system noise include subpixel cloud contamination, nonlinear ice motion (rotation, etc.), and numerical noise in the calculation. These can usually be eliminated by increasing the minimum required correlation value. Unfortunately, "good" vectors will also be eliminated. To preserve "good" vectors with lower correlation values than some "bad" vectors, an additional filter is applied. The "next-neighbor" filter is based on the assumption that feature displacements should contain some spatial auto-correlation. Therefore, if a displacement vector derived for a given pixel is "good", neighboring pixels should also have similar displacement vectors. Our algorithm applies a three-value filter. The first value is the minimum required correlation. The second value is the minimum number of required neighbor pixels with good displacement vectors. The third value defines the maximum allowed x and y displacement of the neighbor vectors with respect to the pixel vector. The near neighbor filter is a consistency requirement often used in spatial mapping exercises.

Edge Location: Input data will include the ice edge isoline, which is the set of image pixels containing the ice edge. The input image is gridded to a horizontal cell by a 3 X 3 aggregation of the pixels. The location of the edge for a given horizontal cell is the mean value of the edge locations in the cell:

$$X_E = \Sigma\ X_i W_i / \Sigma\ W_i \quad (3.3\text{-}15)$$

$$Y_E = \Sigma\ Y_i W_i / \Sigma\ W_I \quad (3.3\text{-}16)$$

Where the summation is over the nine pixels in the cell, and $W_i = 1.0$ if pixel (i) is an edge pixel.

Edge Motion: The ice edge motion for a given cell is then computed as the weighted mean of the neighboring motion vectors, where the neighbor's weight is inverse to the distance between the neighbor and the edge location:

$$(V_X)_E = \Sigma\ (V_X)_j (1. / (R_j - R_E)) / \Sigma\ (1. / (R_j - R_E)) \quad (3.3\text{-}17)$$

$$(V_Y)_E = \Sigma\ (V_Y)_j (1. / (R_j - R_E)) / \Sigma\ (1. / (R_j - R_E)) \quad (3.3\text{-}18)$$

where: $(R_j)^2 = (X_j)^2 + (Y_j)^2$ (3.3-19)

$$(R_E)^2 = (X_E)^2 + (Y_E)^2 \quad (3.3\text{-}20)$$

and the summation is over all motion vectors within a specified distance of R_E.

3.3.4 Archived algorithm output

The retrieved ice age classification for each horizontal cell shall be archived with an associated geo-location.

The retrieved ice edge motion for each horizontal cell shall be archived as a vector with latitude and longitude components, with an associated geo-location.

4.0 EDR PERFORMANCE

The performance of the algorithms with respect to the VIIRS requirements and the System Specification (c.f. Tables 1 and 2) is reviewed in this section.

EDR performance during Phase I of the NPOESS program shall be verified by analysis, modeling, and/or simulation based on the instrument design and performance characteristics and the algorithms. The analysis, modeling, and/or simulation shall be sufficiently extensive in scope to verify that EDR requirements are met under a broad range of conditions that are representative of those occurring in nature, including both typical and extreme conditions.

4.1 STRATIFICATION

4.1.1 Ice Age

Four ice age types are listed in the VIIRS SRD: New, Young, First Year, and Multi-year

Our specification, based on Vis-IR feasibility, is to type a cell containing sea ice as one of three types: New or Young, First Year, or Multi-year. Multi-year ice is all ice that has survived a melt season. New/Young ice is separated from other First Year ice by a thickness threshold of 0.3 meters. Our algorithm classifies ice type by using three methods:

(1) Multi-year ice is distinguished from First Year ice by a filtered distribution of ice reflectance (daytime) or ice temperature (nighttime).

(2) Nighttime discrimination of New/Young ice from thicker First Year ice is achieved by an energy balance derivation of ice thickness from ice temperature.

(3) Daytime discrimination of New/Young ice from thicker First Year ice is achieved by application of a reflectance threshold.

Classification of Multi-year or First Year: Our algorithm takes into account features of spatial changes in ice characteristic values in a local region under consideration. Those characteristics are surface reflectance at daytime and ice surface temperature at nighttime. Changes in the characteristic values are related to different influencing factors. Therefore, we analyze performance of our algorithm for daytime and nighttime separately. Performance of Multi-year / First Year classification strongly depends upon the difference between values of reflectance or surface temperature for those two ice types. We consider the difference between corresponding values as a main stratifying parameter. In addition, we will calculate errors at nadir and edge of scan.

Nighttime Classification of New/Young or First Year: We will calculate errors at nadir and edge of scan.

Daytime Classification of New/Young or First Year: We will calculate errors at nadir and edge of scan

4.1.2 Ice Edge Motion

Ice edge motion is derived from ice concentration and ice edge location. These are stratified by ice concentration truth and by scan angle, as discussed in the VIIRS Imagery ATBD *[Y2466]*. Because ice edge motion is derived from image pairs with no common scan angle, and with a range of ice concentration, it cannot be stratified in the same way. We will summarize non-stratified performance, based on analysis of a MODIS Airborne Simulator image pair, in Section 4.2.2.

4.2 PERFORMANCE ANALYSIS

4.2.1 Ice Age

4.2.1.1 Classification of Multi-year or First Year

Probability of correct typing was verified by demonstration as follows:

TOA Reflectances in the AVHRR visible band were obtained from an AVHRR scene of the Chuckchi Sea. These were used as input to our algorithm. Daytime performance will depend on spatial variability in surface reflectance and on the difference between predominant values of reflectance characteristic for First Year ice and Multi-year ice. The values of predominant reflectances for First Year ice and Multi-year ice types differ more than 0.1 at the scene under consideration. This relatively large difference in reflectance allows us reliably classify pixels on the scene as belonging to one of ice types. That classification was adopted as "truth". Reflectance means and RMS variations were calculated for each type.

The reflectances were then perturbed by the model for Surface reflectance IP error. The errors depend on surface reflectance truth, which is slightly correlated with ice age. Both accuracy and precision errors were applied. Accuracy errors include a modeled calibration bias. Precision errors are derived from the sensor noise. Models for error at nadir and edge of scan were applied. For each scan angle, three test data sets were constructed by offsetting the Multi-year reflectances to simulate mean reflectance differences of 0.05, and 0.075, and 0.1 for the two classes. Classification was performed on each of the six test data sets, and compared to “truth”.

A similar approach we used for assessment of nighttime performance. The difference between predominant values of First Year ice and Multi-year ice was used as a main stratifying parameter. Surface temperatures were perturbed, using model errors for the Surface temperature IP. Accuracy and precision errors were determined by simulation.

We applied the algorithm to the perturbed scenes to retrieve ice age and computed probability of correct typing by comparing the retrieved ice age to the "truth". The deviation between retrieved and true ice age were not aggregated.

The following tables show the probability of correct ice typing stratified by separation between predominant reflectances and temperatures of First Year and Multi-year ice types.

Table 8. Probability of Correct Typing for First Year / Multi-year Ice classification Case 1 (Clear, Day)

Scan Angle	Difference between predominant reflectances		
	0.050	0.075	0.100
Nadir	84%	90%	92%
Edge of Scan	83%	90%	92%

Table 9. Probability of Correct Typing for First Year / Multi-year Ice classification Case 2 (Clear, Night)

Scan Angle	Difference between predominant surface temperatures		
	1 K	1.5 K	2.0 K
Nadir	81%	88%	92%
Edge of Scan	80%	88%	92%

4.2.1.2 Nighttime Classification of New/Young or First Year

All components of the surface energy balance, Equation 3.3.2.1.1, or parameters determining these components, can be directly retrieved from VIIRS and CMIS observations. At the present time, we do not have all necessary information, and need to use an alternative approach for verification.

Analysis of the performance of the energy balance algorithm was made as follows:

Ice thickness is derived from the energy balance equation (3.2.2.1.12). Differentiation of equation 3.2.2.1.12 with respect to each contributing error term yields the analytic dependence of the error in H on each error source. At night, the solar radiation term vanishes, leaving us with three major error sources:

T_s – surface temperature
T_a – surface air temperature
h – snow depth

A typical ice growth season in the vicinity of Barrow, Alaska was modeled, with a climatological history of air temperature and snow depth. Ice thickness error was then derived analytically from estimates of error in air temperature, snow depth, and observed surface temperature. From the distribution of ice thickness and ice thickness measurement error, probability of correct classification is calculated.

Ice temperature does not adjust to changes in air temperature immediately. Due to thermal inertia, ice temperature follows changes in air temperature with a lag of 1 to 12 hours, depending on ice thickness. Thus, the most exact mathematical description of thermal processes in ice cover can be obtained if we combine current ice temperature with average air temperature during the previous 12 hours. This does not degrade algorithm performance. We expect to obtain the

required recent air temperature from CMIS temperature profiles. Our estimate of the baseline error in surface air temperature is 0.6 K. Our estimate is based on our knowledge of CMIS requirements.

Performance also depends strongly on the depth of snow cover on the ice, which varies interannually. Snow depth for a given horizontal cell depends on the precipitation history over the ice in that cell during its growth. We will acquire the estimated ratio of snow depth to ice thickness, based on characteristic precipitation rates and ice growth rates for a given region and season. We adopt an error in snow depth of 0.5 * truth, based on typical variability of these rates.

Ice surface temperature errors are obtained from the specification and performance of the Surface Temperature Intermediate Product (IP). They are 0.578 K (performance at edge of scan (EOS)), and 0.469 K (performance at nadir).

Errors in surface air temperature and snow depth are assumed to be independent of scan angle.

The following tables show the errors stratified by scan angle, snowfall, and ice type. It is assumed that surface air temperature will be available with a measurement uncertainty of 0.6 K.

Table 10. Sea Ice Age Probability of Correct Typing (%)
Case 1: Night, Light Snowfall

Scan Angle	Ice Age Type	
	New or Young	First Year or Multi-year
Nadir	84.1	90.7
Edge of Scan	82.3	89.4

Table 11. Sea Ice Age Probability of Correct Typing
Case 2: Night, Average Snowfall

Scan Angle	Ice Age Type	
	New or Young	First Year or Multi-year
Nadir	77.7	73.7
Edge of Scan	76.2	72.3

Table 12. Sea Ice Age Probability of Correct Typing
Case 3: Night, Heavy Snowfall

Scan Angle	Ice Age Type	
	New or Young	First Year or Multi-year
Nadir	72.1	63.7
Edge of Scan	70.5	62.8

The wide range in EDR performance indicates the sensitivity to snow depth.

4.2.1.3 Daytime Classification of New/Young or First Year

Verification of performance was by analysis. Ice thickness was calculated from a thickness/reflectance relation. Errors in reflectance were acquired from the Surface Reflectance IP error models.

In the absence of error in the thickness/reflectance relation, performance is very good, as shown in Table 13.

Table 13. Sea Ice Age Probability of Correct Typing
Case 1: Day, SZA = 60 degrees

Scan Angle	Ice Age Type	
	New or Young	First Year or Multi-year
Nadir	.986	.958
Edge of Scan	.975	.937

This performance assumes no algorithm error due to an incorrect thickness/reflectance relation. Verification of algorithm errors will require independent sources of ground truth for our simulated data, and must be developed. In the absence of verifiable performance, we will not include daytime retrieval of New or Young vs First year discrimination in our specification. We note that the approach has the potential of being developed into an operational algorithm. The realization of this potential will require the creation of reliable LUTs on ice thickness/reflectance relation.

4.2.2 Ice Edge Motion

The standard approach of deriving ice motion via MCC of features has drawbacks when applied to the marginal ice zones. The persistence of cloud cover during the polar summer interferes with feature identification and results in data gaps during cloudy periods. Cloud cover is often correlated with the ice edge, exacerbating the problem. Effective cloud masking is essential to the success of an MCC technique. The marginal ice zone is a region of large change on time scales of hours to days. Effective ice tracking thus depends on the availability of recent data. This will limit the effectiveness of ice feature tracking with visible-infrared data, unless a reliable cloud mask is available.

Our performance evaluation is based on analysis of one example of a sea ice edge image pair. The scene was obtained by the MODIS Airborne Simulator (MAS) during the FIRE-ACE campaign. Our analysis was performed as follows:

We applied our ice concentration and ice edge location algorithms to the original MAS scenes at 50 meter resolution to establish ice concentration and ice edge location truth. We then aggregated the scenes to a pixel size of 0.2 km, and used these as input to the ice edge motion algorithm. The ice edge motion vectors were computed for each horizontal cell of 1.2 km, representing a VIIRS horizontal cell at nadir.

We then aggregated the MAS scenes to a VIIRS pixel size of 0.4 km at nadir, and perturbed the scenes by our model for surface reflectance error. The resulting scenes were used as input to our ice edge motion algorithm. The RMS deviation between the retrieved ice edge motion vectors and the "true" vectors was calculated.

Figures 3 and 4 illustrates the process:

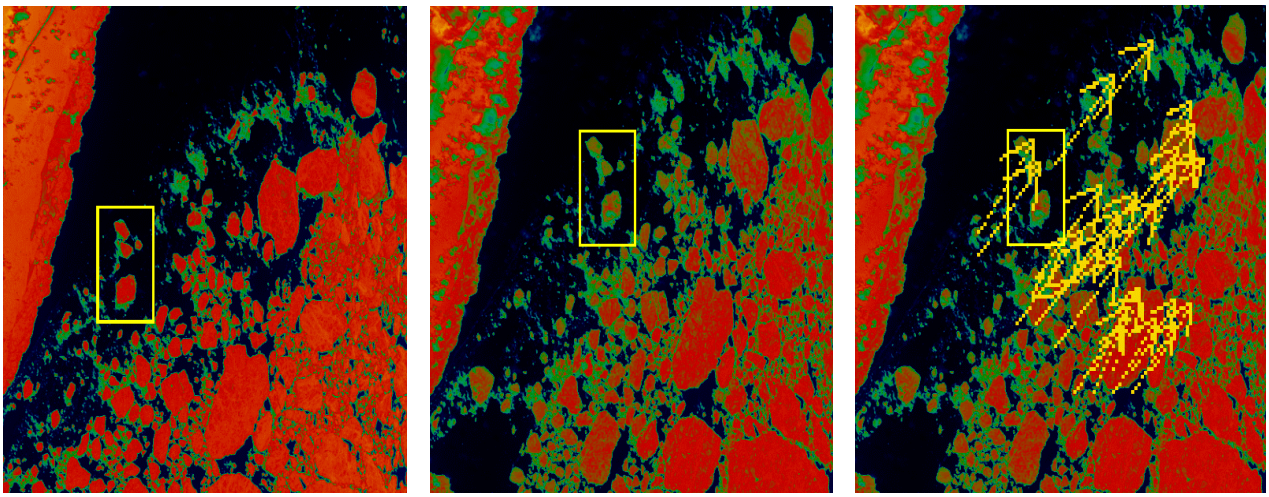

Figure 3. LEFT: Visible reflectance image of the Beaufort Sea, from MODIS Airborne Simulator. The feature on the left side of the image is coastline. The scene is ~25 km by 25 km in extent. CENTER: Image of same scene, 61 minutes later, co-registered with the first scene. The motion of off-shore ice is evident to the eye. RIGHT: The second scene, with ice motion vectors derived by the MCC algorithm. The mean velocity is 110 km/day.

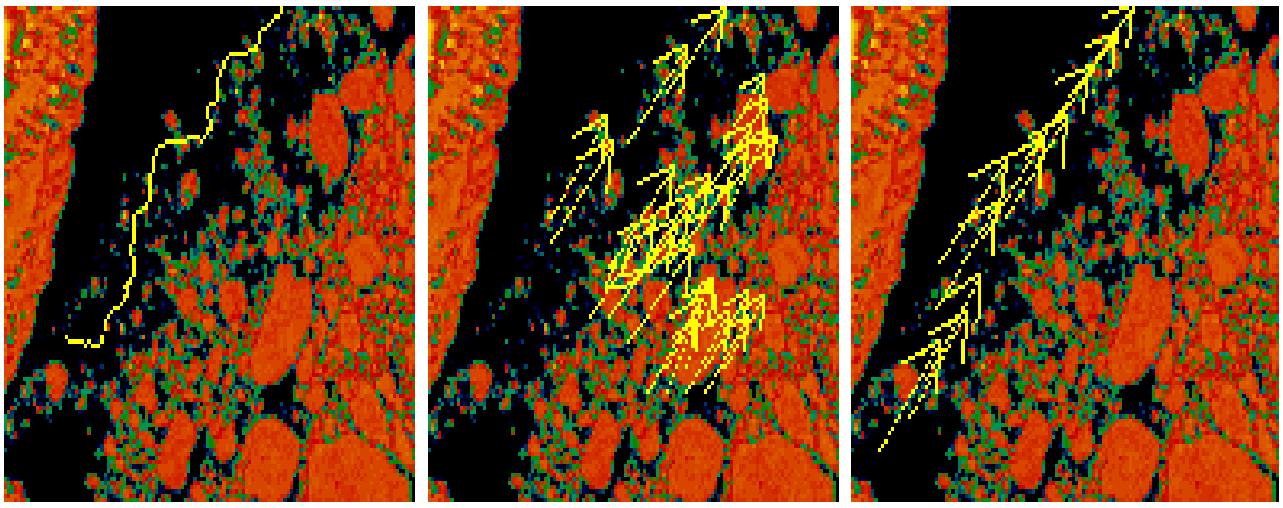

Figure 4. LEFT: The second MODIS Airborne Simulator image of the Beaufort Sea, at VIIRS resolution, with the ice edge location highlighted. CENTER: The same image, with the ice motion vectors highlighted. Ice edge motion vectors are derived by interpolating these vectors to the ice edge location. RIGHT: The resulting ice edge motion vectors, reported for every horizontal cell which contains an ice edge.

Ice edge motion error for our simulation was 3.1 km/day. True motion was 110 km/day for image pairs separated by 1 hour. Scaling to motion of 11 km/day (a more or less typical value) and separations of 10 hours, we would expect an ice edge motion error of 0.31 km/day. We refer to this error as "Ice Concentration". It is expected that the spatial coherence of the scene will degrade over time, resulting in a larger error for a case of 11 km/day motion separated by 10 hours. We make an assumption that the error due to degradation of the scene over a 10 hour period will be equal to the error from ice concentration error. We refer to this error as "Image Coherence". Verification is required to determine how the motion errors will scale with time (c.f. Section 4.4).

Geo-location errors add to the Measurement Uncertainty. The Raytheon VIIRS System Specification for geo-location error is 67 meters at nadir, and 233 meters at edge of scan. Our image pairs will be located with equal probability at any scan angle. We therefore adopt the average value of 150 meters. We assume that the location errors for each image pair are independent, and thus RSS to 212 meters. For a 10 hour separation, this is equivalent to a motion error of 0.51 km/day.

Combining our analysis and assumptions, we derive an ice edge motion error of 0.67 km/day, for typical ice motions separated by 10 hours.

4.2.2.1 Error Budget

The error sources have been assembled into an error budget, shown in Table 14.

Table 14. Error Budget for Sea Ice Edge Motion

SEA ICE EDGE MOTION **Specification v3 (PDR)** **04/14/00**	**Case:** **Measurement Uncertainty (km/day)**	**Clear, SZA = 60 degrees,** **10 Hour Separation of Image Pairs** **Reference**
Threshold	1.00	VIIRS SRD
Objective	0.10	VIIRS SRD
System Specification	0.80	Raytheon VIIRS Specification v3
System Performance	0.67	This document, Section 4.2.2
System Margin	0.43	
Ice Concentration	0.31	This document, Section 4.2.2
Image Coherence	0.31	This document, Section 4.2.2
Geo-Location	0.51	This document, Section 4.2.2

4.2.3 Conditions Under Which the Specification Cannot be Attained

Cloudy: VIS/IR retrievals are not feasible under cloudy conditions. The VIIRS Cloud Mask will mask cloudy pixels. Cloud error assessment will require an analysis of cloud masking

performance over ice surfaces. Cloud-masked gaps in the images can be a hindrance to correlation methods. The problem is mitigated by the application of an accurate cloud mask, and the de-weighting of pixels which are cloud masked in either member of the image pair.

Small difference between predominant values of reflectances or temperatures characteristic for First Year and Multi-year ice types: The algorithm performance will not meet specification if the difference between reflectances is less than 0.042 and between temperatures is less than 1K.

Heavy Snowfall (New or Young vs First Year): If recent snowfall has been greater than 6 cm/month, snow depth errors will degrade performance of the energy balance algorithm.

Low Light During Summer: A reliance on solar reflectance bands suffers from limitations during low light conditions. A solar zenith angle threshold will be applied to flag pixels with suspect quality due to low light. We expect that atmospheric correction error will drive the setting of a solar zenith angle threshold. The threshold will depend on region and season, as atmospheric conditions dictate.

Low thermal contrast at night: The thermal contrast between ice and open water is too low during the summer and part of other seasons to allow for ice age and ice edge location derivations from thermal bands.

4.3 PRACTICAL CONSIDERATIONS

4.3.1 Numerical computation considerations

The requirement to retrieve EDRs on a global, operational basis in a 20 minute time frame places no constraints on our ice age algorithms. Our technique is not computationally intensive. A constraint on the template and search window sizes for ice edge motion is often necessary to reduce the computational load. The constraint can be largely relaxed by software modifications, as was demonstrated for the search window method of the ice concentration algorithm *[Y2466]* .

4.3.2 Programming and procedural considerations

All procedures must be automatic to perform in the operational environment. We expect that the algorithm will be directed by decision nodes, based on availability and quality of data and regional, seasonal considerations. Therefore, all required LUTs must be available at all times.

4.3.3 Configuration of retrievals

The Sea Ice Age algorithm expects the output from the VIIRS Ice Concentration Imagery ARP and the VIIRS Ice Edge Location Imagery ARP. The EDR output is not needed as input ancillary data for any other VIIRS EDRs. The NPOESS processing configuration should be designed to satisfy these expectations.

The Sea Ice Edge Motion algorithm expects the output from the VIIRS Ice Concentration Imagery ARP and the VIIRS Ice Edge Location Imagery ARP. The EDR output is not needed as input ancillary data for any other VIIRS EDRs. The NPOESS processing configuration is designed to satisfy these expectations.

4.3.4 Exception Handling

Pixels identified by the cloud mask will be skipped. Pixels with bad quality flags will be skipped and flagged. Bands with bad quality flags will be removed.

4.4 INITIALIZATION AND VALIDATION

4.4.1 Initialization

Initialization and validation activities shall be coordinated with the National Ice Center, with the purpose of assuring that the VIIRS data products can be incorporated into their strategic product.

Our plan is to establish and maintain close contact with the MODIS teams, following the selection phase of the NPOESS program, to coordinate our initialization activity with their post-launch validation.

Polar atmosphere models including an Arctic haze component will be applied to large solar zenith data to optimize the models for polar conditions, and to develop decision rules for solar zenith angle thresholds. MODIS data taken at solar zenith angles greater than 70 degrees will be studied to fine tune our solar zenith angle threshold for daytime conditions. The limiting factor is believed to be the reliability of atmospheric correction at larger solar zenith angles. Plane parallel radiative transfer algorithms are inaccurate for angles greater than 70-75 degrees. Development of improved radiative transfer models at larger angles will allow us to relax this constraint. To solve the Radiative Transfer Equation appropriately one would have to take into account the spherical shell atmosphere geometry (Thomas and Stamnes, 1998). It is expected that “truth” can be established from *in situ* data obtained from MODIS validation campaigns.

MODIS Airborne Simulator (MAS) observations will be used to optimize cloud detection over snow surfaces. The VIIRS Cloud Mask will be applied over a series of MAS images for which there are varying degrees of snow cover to evaluate and optimize its performance.

Creation of snow depth LUTs will be accomplished from regional/seasonal climatological histories of snow precipitation and air temperature, to support nighttime discrimination of New or Young ice from First year ice.

Creation of thickness/reflectance LUTs will support daytime discrimination of New or Young ice from First year ice.

Analysis of sea ice age algorithm performance with MODIS data will be used to determine relative weights of the visible and NIR bands, if we can establish ice age “truth” from MODIS validation data. In that case, simulated VIIRS scenes in visible and NIR will be generated from the MODIS data, which contains similar bands. Band weights will be optimized to provide the best match of simulated VIIRS retrievals to MODIS “truth”.

Optimization of search window and filter parameters for ice edge motion will be developed from MODIS data. The effect of mixed cloud cover in the image pairs will be analyzed, with the intention of developing a threshold maximum fraction of cloud cover in a search region. A quality flag can be attached to a retrieval from an image pair with a fraction of cloud cover

greater than the threshold. Alternatively, a recent CMIS image can be used when all recent VIIRS images have cloud cover above threshold.

4.4.2 Pre-Launch Characterization

The pre-launch plan for the Sea Ice Age and Sea Ice Edge Motion EDR includes sensitivity studies, analysis of simulated VIIRS data, and verification using MODIS-type data. Observations from AVIRIS, MAS, MODIS, GLI, and NPP will be used in the pre-launch phase to study the error characteristics and optimum techniques for the algorithm. It is expected that MODIS validation data will be of great value. This data is expected to include *in situ* field measurements combined with MODIS observations, MAS underflights, and low level aircraft measurements at spatial resolutions less than 10 meters. Our plan is to use this data in combination with the VIIRS sensor model to produce simulated VIIRS scenes, apply our algorithms to retrieve our EDR products, and compare our results with "truth" derived from *in situ*, aircraft, and MAS data.

The potential for VIIRS/CMIS data fusion to produce First Year/Multi-year classification and ice edge motion will be studied with the use of MODIS data and AMSR data.

Buoy data will be used to establish "truth" for ice edge motion. Buoys can be used in the deeper pack ice to characterize the performance of the MCC method. Use of buoys will be limited in the MIZ, but would be of special value for performance analysis near ice edges.

4.4.3 Validation

Our pre-launch plan is designed to interface smoothly with post-launch validation activity. We would propose to conduct a post-launch VIIRS validation campaign similar to the MODIS validation activity. In this sense, post-launch validation will already have been simulated by the pre-launch activity. Following launch, we would substitute real VIIRS data for the pre-launch simulated data. We would establish "truth" by the same process.

We expect our pre-launch MODIS/AMSR validation activity to merge smoothly with VIIRS/CMIS validation. We expect that MODIS/AMSR ground truth resources will be maintained for the VIIRS post-launch validation.

5.0 ASSUMPTION AND LIMITATIONS

5.1 ASSUMPTIONS

The statements and conclusions in this document are subject to the validity of the following assumptions:

(1) An effective cloud mask over snow and ice surfaces will be available from the VIIRS Cloud Mask IP *[Y2412]*.

(2) Surface reflectances, brought to standard conditions, will be derived from TOA radiances and supplied as a Surface Reflectance IP *[Y2411]*, with errors as specified in the VIIRS System Specification *[PRF SS 154640-001]*

(3) Surface temperatures, will be derived from TOA radiances and supplied as a Surface Temperature IP *[Y2405]*, with errors as specified in the VIIRS System Specification *[PRF SS 154640-001]*

5.2 LIMITATIONS

The following limitations apply to the algorithms described in this document:

Clear conditions only. The definition of "clear" will be developed in coordination with the development of the VIIRS Cloud Mask IP *[Y2412]*. It will depend upon the capability of the cloud mask over snow and ice surfaces and upon the capability of radiative transfer modeling through thin clouds.

6.0 REFERENCES

Agnew, T.A., H.Le, and T. Hirose, "Estimation of large-scale sea-ice motion from SSM/I 85.5 GHz imagery," *Ann. Glaciology, 25*, 305-311, 1997.

Boardman, D. *et al*., "Development of a sea-ice workstation for the automated monitoring of sea ice," *Polar Record*, 31(177), 155 – 160, 1995.

Bohren, C.F., and B.R. Barkstrom (1974). Theory of the optical properties of snow. *J. Geophys. Res.*, 79, 4527-4535.

Bolsenga, S.J., "Spectral reflectances of snow and fresh-water ice from 340 through 1100 nm," *J. Glaciology*, 29(102), 296-305, 1983.

Bromwich, D.H. and Tzeng, R.-Y., "Simulation of the modern arctic climate by the NCAR CCM1," *J. Climate***,** 7, 1050-1069, 1994.

Crane, R.G. and M.R. Anderson (1984). Satellite discrimination of snow/cloud surfaces. *Intl. J. Remote Sens*., 5(1), 213-223.

De Abreu, R.A., D.G. Barber, K. Misurak, and E.F. LeDrew, "Spectral albedo of snow-covered first-year and multi-year seaice during spring melt," *Ann. Glaciology, 21*, 337-342, 1995.

Domingues, C.M. G.A. Goncalves, R.D. Ghisolfi and C.A.E. Garcia, 1999, Advective surface feclosities derived from sequential infrared images in the southwestern atlantic ocean, submitted to *J. Rem. Sens. Envi.*

Dozier, J. (1984). Snow reflectance from Landsat-4 Thematic Mapper. *IEEE Trans. Geosci. Remote Sens.*, 22(3), 323-328.

Dozier, J. (1989). Spectral signature of alpine snow cover from the Landsat Thematic Mapper. *Remote Sens. Environ*., 28, 9-22.

Emery, W. J., Radebaugh, M., and Fowler, C. W., "A comparison of sea ice parameters computed from AVHRR and Landsat satellite imagery and from airborne passive microwave radiometry," *J. Geophys. Res.,* 96(C12), 22,075 – 22,085, 1991.

Eppler, D.T., Farmer, L.D., Lohanick, A.W. *et al.*, "Passive microwave signatures of sea ice," in Micowave Remote Sensing of Sea Ice, Geophysical Monograph 68, American Geophysical Union, 47-71, 1992.

Grenfell, T.C., D.K. Perovich, and J.A. Ogren (1981). Spectral albedos of an alpine snowpack. *Cold Regions Sci. Technol*., 4, 121-127.

Grenfell, T.C. and G. Maykutt, "The optical properties of ice and snow in the Arctic Basin, *J. Glaciology, 18*, 445-463, 1977.

Hall, D.K., Foster, J.L., Chang, A.T.C., and Rango, A., "Freshwater ice thickness observations using passive microwave sensors," *IEEE Trans. Geosci. Remote Sens.*, GE-19(4), 189-193, 1981.

Hall, D.K., Fagre, D.B., Klasner, F., Linebaugh, G., and Liston, G.E., "Analysis of ERS-1 synthetic aperture radar data of frozen lakes in northern Montana and implications for climate studies," *J. Geophys. Res.*, 99(C11), 22,473-22,482, 1994.

Hucks, J., SBRS Ref:Y1629, March 4, 1998.

Jeffries, M.O., Morris, K., and Weeks, W.F., "Structural and stratigraphic features and ERS-1 synthetic aperture radar backscatter characteristics of ice growing on shallow lakes in NW Alaska, winter 1991-1992," *J. Geophys. Res.*, 99(C11), 22,459-22,471, 1994.

Kwok, R., A. Schweiger, D.A. Rothrock, S. Pang, and C. Kottmeier, "Sea ice motion from satellite passive microwave imagery assessed with ERS SAR and buoy motions," *J. Geophys. Res., 103*, 8191-8214, 1998.

Lee, J.S. and I. Jurkevich, "Segmentation of SAR images," *IEEE Trans. On Geoscience and Remote Sensing, 27,* 674-680, 1989.

Lee, J.S., "A simple speckle smoothing algorithm for synthetic aperture radar images," *IEEE Trans. On Systems, Man, and Cybernetics, 13,* 85-89, 1983.

Lindsay, R. and Rothrock, D., "The calculation of surface temperature and albedo of Arctic sea ice from AVHRR," *Ann. Glaciology*, 17, 1993.

Liu, A.K., Y. Zhao, and S.Y. Wu, "Arctic sea ice drift from wavelet analysis of NSCAT and special sensor microwave imager data," *J. Geophys. Res., 104, No.C5,* 11529-11538, 1999.

Loset, S. and Carstens, T., "Sea ice and iceberg observations in the western Barents Sea in 1987," *Cold Regions Science and Technology*, 24, 323 – 340, 1996.

Lythe, M., A. Hauser, and G. Wendler, "Classification of sea ice types in the Ross Sea, Antarctica from SAR and AVHRR imagery," *Int. J. Remote Sensing, Vol.20, No 15 & 16,* 3073-3085, 1999.

Massom, R. and Comiso, J.C., "The classification of Arctic sea ice types and the determination of surface temperature using AVHRR data," *J. Geophys. Res.*, 99(C3), 5201-5218, 1994.

Ninnis, R. W., Emery, W. J., and Collins, M. J., "Automated extraction of pack ice motion from AVHRR imagery," *J. Geophys. Res.*, 91(C9), 10,725 – 10,734, 1986.

Partington, K. C. and Steffen, K., "Proposed development of a joint scientific-operational Arctic-wide sea ice product," National Ice Center White Paper, 1998.

Smith, D.M., E.C. Barret, and J.C. Scott, "Sea ice type classification from ERS-1 SAR databased on gray level and texture information," *Polar Record, 31,* 135-146, 1995.

Thomas, G. and Stamnes, K., "Radiative Transfer in the Atmosphere and Ocean," textbook, in press, Cambridge Atmospheric and Space Sciences Series, 1998.

Thorndike, A.S., "Kinematics of sea ice," in *The Geophysics of Sea Ice*, N. Untersteiner (ed.), Plenum, New York, 1986.

Warren, S.G., "Optical properties of snow," *Rev. Geophys. Space Phys.*, 20(1), 67-89, 1982.

Warren, S.G., and W.J.Wiscombe (1980). A model for the spectral albedo of snow.II. Snow containing atmospheric aerosols, *J. Atmos. Sci.*, 37(12), 2734-2745.

Wiscombe, W.J., and S.G. Warren (1980). A model for the spectral albedo of snow,1,pure snow. *J. Atmos. Sci.*, 37(12), 2712-2733.

Yu, Y. and Rothrock, D.A., "Thin ice thickness from satellite thermal imagery," *J. Geophys. Res.*, 101(C10), 27,753 – 25,766, 1996.